Brazilian Journal
of Chemical
Engineering

ISSN 0104-6632
Printed in Brazil
www.abeq.org.br/bjche

Vol. 33, No. 01, pp. 73 - 90, January - March, 2016
dx.doi.org/10.1590/0104-6632.20160331s20140016

THE EFFECT OF SYSTEM TEMPERATURE AND PRESSURE ON THE FLUID-DYNAMIC BEHAVIOR OF THE SUPERCRITICAL ANTISOLVENT MICRONIZATION PROCESS: A NUMERICAL APPROACH

R. A. Almeida[1*], R. V. P. Rezende[2], V. F. Cabral[1], D. Noriler[3], H. F. Meier[3], L. Cardozo-Filho[1] and F. A. R. Cardoso[4]

[1]Department of Chemical and Food Engineering, State University of Maringa, 87020-900, Maringá - PR, Brazil.
Phone: + 55 (44) 30253034; + 55 (44) 98897070
E-mail: regiani_al@hotmail.com
[2]Department of Chemical and Food Engineering, Federal University of Santa Catarina,
88040-970, Florianópolis - SC, Brazil.
[3]Department of Chemical Engineering, Regional University of Blumenau,
89030-000, Blumenau - SC, Brazil.
[4]Department of Mathematics, Federal Technological University of Paraná,
87301-005, Campo Mourão - PR, Brazil.

(Submitted: August 25, 2014 ; Revised: February 25, 2015 ; Accepted: March 19, 2015)

Abstract - The Supercritical Antisolvent (SAS) technique allows for the precipitation of drugs and biopolymers in nanometer size in a wide range of industrial applications, while guaranteeing the physical and chemical integrity of such materials. However, a suitable combination of operating parameters is needed for each type of solute. The knowledge of fluid dynamics behavior plays a key role in the search for such parameter combinations. This work presents a numerical study concerning the impact of operating temperature and pressure upon the physical properties and mixture dynamics within the SAS process, because in supercritical conditions the radius of the droplets formed exhibits great sensitivity to these variables. For the conditions analyzed, to account for the heat of mixture in the energy balance, subtle variations in the temperature fields were observed, with almost negligible pressure drop. From analyses of the intensity of segregation, there is an enhancement of the mixture on the molecular scale when the system is operated at higher pressure. This corroborates experimental observations from the literature, related to smaller diameters of particles under higher pressures. Hence, the model resulted in a versatile tool for selecting conditions that may promote a better control over the performance of the SAS process.
Keywords: Supercritical Antisolvent; Nanoparticles; Mathematical modeling; Intensity of segregation; CFD.

INTRODUCTION

The supercritical state of a mixture is obtained when its temperature and pressure are above their critical values. Techniques for the production of micro- and nanoparticles using supercritical fluids (SCF) have been modified and explored towards diverse applications, including the pharmaceutical,

*To whom correspondence should be addressed

cosmetics, and food industries as alternatives to traditional fine powder production.

Among such techniques, one can highlight: the RESS - Rapid Expansion of Supercritical Solutions technique and its variants such as RESOLV, RESSAS (Türk and Bolten, 2010), and the SAS technique (Supercritical Antisolvent) and some variants such as SEDS, GAS and PCA (Bałdyga *et al*., 2010; Jerzy *et al*., 2004; Martín *et al*., 2007).

In the RESS techniques, the solute must be soluble in the supercritical fluid (SCF). They are characterized by a pre-expansion chamber where the mixture of solute and the SCF are pressurized and then expanded through a convergent-divergent nozzle causing a sudden pressure drop and the precipitation of the solute.

The SAS technique, which is the object of this study, is used as an alternative when the solute of interest is not soluble in the SCF and such technique requires that the organic solvent possess a greater affinity for the antisolvent than for the solute. This technique generally makes use of CO_2 and allows the processing of a large variety of high quality industrial products (Martín *et al*., 2007; Sanguansri and Augustin, 2006). An organic solution of solvent/solute and the CO_2 enter continuously through a coaxial capillary into a pressurized precipitation chamber pre-charged with antisolvent (CO_2). The solution interacts with the antisolvent, increasing the diffusion in the organic antisolvent mixture and causing the precipitation of the solute.

Among its applications, we highlight the development of biomedical materials based on prolonged liberation mechanisms, such as nanoencapsulation applied to vaccine production, allergy and even cancer treatment, e.g. (Balcão *et al*., 2013; Cushen *et al*., 2012).

In a supercritical mixture, physical properties such as density, and thermodynamic parameters such as solubility may be adjusted within a wide range of processing conditions through varying pressures, flow rate, and temperatures. The rapid transfer of mass that occurs upon injecting a solution into a fluid such as CO_2 under supercritical conditions is characterized by an elevated diffusivity and low viscosity. Such characteristics are considered beneficial to precipitating tiny spherical particles from the solute (on a nanometric scale) and necessary for their industrial application.

There are several key operational SAS parameters such as: solution and antisolvent flow rates; injection capillary length and diameter; chamber geometry; operational pressure and temperature (T_0 and P_0); these last two have been reported in the literature as being of special importance. More specifically, near the critical point of the mixture, the droplets formed exhibit high sensitivity to the thermodynamic coordinates T_0 and P_0, which have great influence on the morphological changes of the precipitated substances (Reverchon *et al*., 2008; Werling and Debenedetti, 2000).

With respect to the variation of particle size, contradictory behavior can be found in the relevant literature. For example, increased operational pressure of the system may result in gains (Franceschi, 2009), losses (Miguel *et al*., 2006), or in practically no noticeable impact upon the precipitated particles (Chang *et al*., 2008). As to increases in operational temperature, some solutes diminish in size while others expand. These discrepancies among results depend on the physical nature of the solute and require further and more profound study (Erriguible *et al*., 2013b).

Modulation of the operating pressure and temperature directly influences the variation of density. In turn, this influences the dimensions or the sizes of the precipitated particles, which thus depend upon the differences in density between regions rich in organic solvent and CO_2-rich regions.

Concerning density differences, Werling and Debenedetti (2000) utilized toluene as an organic solvent and CO_2 as an antisolvent and reported an increase in size of the particles when the solvent is denser than the antisolvent; otherwise, the particles decrease in size. This indicates a faster mass transfer from the solution to the surrounding CO_2.

Some published studies have intended to evaluate the impact of thermodynamic coordinates on precipitated particle size (Franceschi, 2009; Franceschi *et al*., 2008; Imsanguan *et al*., 2010; Lengsfeld *et al*., 2000; Martín and Cocero, 2008; Miguel *et al*., 2006; Reverchon and De Marco, 2011). In their majority, they are experimental and designed for solute systems with specific physical-chemical properties. They are also designed for experimental adequacy to obtain good T_0 and P_0 limits for a determined system (for particular combinations of solutes and organic solvents), given the time expended to carry out several experimental runs and high material costs (Erriguible *et al*., 2013b). Beyond this, under high pressure, optical measurements to observe the flow patterns (as shadowgraphs or schlieren techniques) of the precipitation process may be obscured by temperature gradients, species concentration, and large

numbers of very small particles that accompany flow in the precipitation chamber (Jerzy *et al*., 2004). This changes the way in which light passes through the flow, since the density variation may interfere with refractive indices and cause delay associated with non-homogeneity in the mid-section (Raffel *et al*., 1998).

Experimentally, with respect to the influence of T_0 and P_0 upon the size and formation of particles, one knows that: increased temperature keeping all other variables constant (solvent and CO_2 flows, pressure, and chamber geometry) increases the tendency to agglomerate; irregular particles (Boschetto, 2013), expanded microparticles and fibers, as well as increased particle size prevail (Reverchon and De Marco, 2011). It has also been shown that pressure increases favor obtaining smaller sized particles and a narrower distribution of sizes, given that, with increased pressure, the intermolecular distances diminish, in turn augmenting CO_2 density (*viz*. Table 1). The difference in density between pure ethanol and pure CO_2 decreases which results in a better mixture between the solution and the SCF, forming smaller particles (Boschetto, 2013; Franceschi *et al*., 2008; Reverchon *et al*., 2007). Contradictorily, according to Franceschi (2009) the increased pressure can result in larger particles when low levels of solvent and CO_2 flow rate are considered, as well as low initial concentration of solute in the organic solvent.

Thus, given the experimental complexity, the use the numerical simulation arises as a suitable alternative to determine the influence of operational parameters in the fluid dynamic behavior of flows within the SAS process, increasing its performance. This is an innovative approach concerning the FSC precipitation process, and it demands low cost and has the advantage of obtaining satisfactory results over a short time period (Bałdyga *et al*., 2010; Martín and Cocero, 2004; Sierra-Pallares *et al*., 2012; Werling and Debenedetti, 2000).

The numerical studies employing Computational Fluid Dynamics (CFD) seek to find appropriate conditions for spherical particle precipitation on a nanometric scale (Bałdyga *et al*., 2010; Cardoso *et al*., 2008; Erriguible *et al*., 2013b). However, within this scope there remains a lack of specific publications referring to the influence of operational temperature and pressure parameters upon the dynamics of the supercritical mixture. Some authors do consider the SAS process in the isothermal regime (Cardoso *et al*., 2008; Erriguible *et al*., 2013a; Martín and Cocero, 2004), while others have emphasized the influence of temperature variation (Jerzy *et al*., 2004; Sierra-Pallares *et al*., 2012).

In this sense, Martín and Cocero (2004) describe the SAS process according to a two-dimensional isothermal regime approach, modeling it as a turbulent mixture employing the standard k-ε turbulence model of completely miscible fluids, coupled to a model that predicts particle growth. In so doing, they evidenced that the flow rates and the mixture dynamics strongly influence the precipitation that occurs in an environment of great compositional variance.

Sierra-Pallares *et al*. (2012) also proposed a two-dimensional and non-isothermal mathematical model coupled with a populational balance equation (PBE) associated with a closure model for the micromixing to describe particle sizes of *β*-carotene and concluded that temperature is quickly homogenized upon capillary exit. In that region there is approximately 4 K of variation; the flow pattern near the capillary exit is determined by the solution injection velocity; and the vortex generated in this region promotes the formation of intense mixture and is responsible for the mixture on macro scales.

Based on a non-isothermal approach coupled with a PBE and comparing with experimental data, Henczka and Shekunov (2005) pointed out the importance and better accuracy of models to predict particles sizes that consider the micro-mixing when compared to simulations that do not consider this physical process.

According to Erriguible *et al*. (2013b) in their study on the influence of pressure in subcritical conditions, increasing pressure has moderate impacts upon viscosity and significant impacts upon mixture density. They conjecture that this effect tends to remain under supercritical conditions. However, there are works in computational simulation which have modeled the SAS process in an incompressible regime (Cardoso *et al*., 2008; Erriguible *et al*., 2013a). Thus, the compressibility of the mixture in the process, as well as the impacts of pressure and temperature upon physical properties and flow patterns, has not yet been sufficiently examined and outlined.

In the cited numerical studies, there is no reference to modeling of the physical properties of the mixture, except Cardoso *et al*. (2008) who consider the dependence of the viscosity with the mass fractions of the solvent and the antisolvent; Sierra-Pallares *et al*. (2012) employed the method of Chung *et al*. (1988) for the thermal conductivity and the viscosity and the method of He and Yu (1998) for the diffusivity. However, there are no reports about the

influence of these assumptions on the flow dynamics or the size of the precipitated particles.

In particular, small diameter particle precipitation is directly associated with low viscosity (Bałdyga *et al*., 2010), and high levels of mixture diffusivity and thermal conductivity is required for proper thermal fields (Yamamoto *et al*., 2011). Thus, given the lack of relevant literature references concerning this aspect, it becomes important to investigate the influence of T_0 and P_0 upon these properties.

Given viscosity, thermal conductivity, and the diffusivity coefficient in the region near the Critical Point of the Mixture (CPM) as well as where $1 < Tr_m < 1.5$ and $P > Pc_m$ (as the conditions considered in this study), pressure exerts an effect on the mixture viscosity, which may diminish with increased temperatures. Increases in thermal conductivity in the supercritical mixture also showed themselves to be particularly sensitive to increases in pressure and diminished with temperature increases. The diffusivity coefficient is significantly affected by variations in mixture composition and high pressures with respect to the ideal gas condition (Poling *et al*., 2004). Thus, in typical supercritical conditions, it is important to investigate if the fluidynamic modeling of the SAS process requires consideration of adequate models in order to describe the mixture's physical properties.

In this work a mathematical model is presented to describe the SAS process fluid dynamics coupled to the turbulence model k-ε. Initially, based on Peng-Robinson's cubic equation solution, this study presents the density dependence of the mixture with respect to incremental pressure and temperature variations around their operational values. Then, based on the model's solution, the influence of values P_0 and T_0 on transport properties and upon the dynamic of flow of the binary mixture of CO_2 and ethanol was analyzed. In such analysis, the process is operated in the region of the phase diagram above CPM. In this region the mixture is found as a single phase. Finally, analysis is provided concerning the sensitivity to T_0 and P_0 on a molecular level.

METHODOLOGY

The model is represented by the system of Equations (1)-(19) in order to describe the flow from the SAS process in steady state, considering it as compressible, non-isothermal, and in the turbulent regime because the transition from a laminar jet to a turbulent jet occurs at low Reynolds numbers (Silveira-Neto, 2002). Under the conditions considered in this study: $Re \simeq 300$ for the ethanol inlet and $Re \simeq 1500$ for the CO_2 inlet. ANSYS FLUENT 13.0 software was used to solve the system of equations. The chamber utilized in this study has cylindrical geometry and couples with a capillary tube in the center of the lid in a coaxial system in order to inject the ethanol and CO_2. A two-dimensional axis-symmetric approach was considered due to the geometric circumferential symmetry, with a non-uniform cartesian mesh composed of 115.5 thousand of elements. A preliminary comparison with a three-dimensional approach employing a tetrahedral mesh with approximately 4.2 million elements presented a prohibitive computational effort in a serial run due to computational time. In a parallel run, with 5 partitions of a cluster, it took almost 90 hours when compared with the two-dimensional mesh, which took 16 hours in a serial run on a single Intel Core-i5@2.5GHz CPU and 4GB of RAM memory.

Equation of State PVT

The density of the CO_2 and ethanol mixture was described by the Peng-Robinson equation of state (PREOS), employing the van der Waals quadratic mixing rule.

$$P = \frac{RT}{V - b_m} - \frac{a_m}{V\left(V + b_m\right) + b_m\left(V - b_m\right)}, \tag{1}$$

where P is the absolute pressure, V [m^3 mol^{-1}] is the molar volume, T is the temperature, a_m and b_m are the PREOS mixing parameters calculated using the following rule of mixture:

$$\begin{aligned} a_m &= \sum_i \sum_j y_i y_j a_{ij}, \\ b_m &= \sum_i \sum_j y_i y_j b_{ij}, \end{aligned} \tag{2}$$

where $i, j \in \{1,2\}$, y_i is the mole fraction of component i and the parameters a_{ij} and b_{ij} are calculated using the following combination rules:

$$\begin{aligned} a_{ij} &= \sqrt{a_i a_j}\left(1 - k_{ij}\right), \\ b_{ij} &= \frac{\left(b_i + b_j\right)\left(1 - l_{ij}\right)}{2}, \end{aligned} \tag{3}$$

k_{ij} and l_{ij} are the binary interaction parameters. Here, the following literature values obtained from (Franceschi, 2009) were used: k_{12}=0.0703 and l_{12}= -0.0262. In the above equations, a_i and b_i are the parameters of the pure species. These parameters were determined using:

$$a_i(T) = \frac{0.45723553 R^2 Tc_i^2 \alpha_i}{Pc_i}, \qquad b_i = \frac{0.07779607 Tc_i}{Pc_i}, \tag{4}$$

with

$$\alpha_i(T) = \left[1 + k_i\left(1 - \sqrt{Tr_i}\right)\right]^2, \qquad k_i = 0.37464 + 1.54226\omega_i - 0.26993\omega_i^2, \tag{5}$$

where Tc and Pc are the critical temperature and pressure of species i, respectively; $Tr_i = T/Tc_i$ is the reduced temperature; and ω_i is the acentric factor of species i.

Viscosity

Each component's viscosity was calculated for each T_0 and P_0 as displayed in Table 1 based on Chung's rule as described by Chung *et al*. (1988). Chung's method takes density and high pressures into consideration. The mixing rule given by Equation (6) (Bałdyga *et al*., 2010) was employed in order to obtain the mixture viscosity.

$$\mu_m(T,P) = \left(\mu_{CO_2}\right)^{y_{CO_2}} \left(\mu_{ethanol}\right)^{y_{ethanol}} \tag{6}$$

Thermal Conductivity

To calculate the thermal conductivity of the mixture, $k_m\,[W\,m^{-1}K^{-1}]$, Chung's method was used (Chung *et al*., 1988), as it considers density at high pressures and viscosity at low pressures:

$$k_m(T,P) = \frac{31{,}2\mu^0\psi}{M}\left(\frac{1}{G_2} + Ay\right) + qBy^2 Tr^{1/2} G_2, \tag{7}$$

where M is the molecular weight of the mixture, $\mu^0[Pa.s]$ is the low pressure viscosity; ω_m the acentric factor of the mixture and c_v is the heat capacity at constant volume; R is the universal constant for gases; $y = Vc/6V$ with Vc being the critical volume of the mixture in [cm^3 mol^{-1}]. The factors $\psi = \psi(c_v, R, \omega_m, T, T_c)$, $q = q(T_c, M, V_c)$, $G_2 = G_2(y, D_i)$ are correction functions described in Chung *et al*. (1988), and D_i are functions dependent on the mixture's acentric factor, as well as a correction factor for polar substances as described in Poling *et al*. (2004).

Diffusivity

According to Riazi-Whitson's equation (Riazi and Whitson, 1993), one can determine the diffusivity coefficient. This relationship, which considers viscosity of the mixture μ_m as in Eq. (6), density of the mixture at low ρ^0 and density of the mixture at high pressures ρ, is given by:

$$D_{1,2}(T,P) = 1.07\frac{\left(\rho^0 D^0\right)}{\rho}\left(\frac{\mu_m}{\mu_m^0}\right)^{b+cP_{rm}}, \tag{8}$$

where $b = -0.27 - 0.38\omega_m$ and $c = -0.05 + 0.1\omega_m$, $Pc_m = x_1 Pc_1 + x_2 Pc_2$ and $\omega_m = x_1\omega_1 + x_2\omega_2$. Here x_1 and x_2 are the mole fractions of ethanol and CO_2, respectively. Also, in Eq. (8) Pc_m is the critical pressure of the mixture, D^0 is the diffusivity coefficient of the mixture at low pressure. For simplicity, the mixture density at high pressures was established using Eq. (1), setting the operational pressure and the temperature to be T_0 and P_0 for each case of Table 1 and varying the mixture composition. Then, each case was described by a sixth-degree polynomial as a function of the CO_2 mole fraction obtained by polynomial interpolation.

Governing Transport Equations

With the intent to describe the SAS process, a model based on the mass-weighted Reynolds-averaged Navier-Stokes equations (RANS) was proposed. Some fundamental assumptions can be taken into account to correctly describe the fluidynamics of the formed jet and the mass transfer:

- the supercritical fluid phase under turbulence conditions can be represented by the mass-weighted Reynolds-averaged Navier-Stokes equations (mass-weighted RANS);
- the compressible flow can be analyzed under steady-state;

- there is a complete miscibility between the organic solvent and antisolvent;
- the eddy viscosity hypothesis is assumed;
- energy and chemical species balance equations were included;
- a Newtonian fluid was considered.

It is convenient for compressible flow, to consider the density-weighted Favre average. Given a ϕ flow variable, one considers $\tilde{\phi}(x) \equiv \frac{\overline{\rho\phi(x)}}{\overline{\rho}}$, where $\overline{\rho}$ represents the Reynolds temporal average for density. The field variable can be decomposed as the sum of its mean value and its fluctuation $\phi = \tilde{\phi} + \phi'' = \overline{\phi} + \phi'$ (Wilcox, 1993), Based on the hypotheses presented above, the conservation equations are given as follows:

Continuity Equation

$$\frac{\partial\left(\overline{\rho}\widetilde{u_i}\right)}{\partial x_i} = 0, \tag{9}$$

where ρ represents the density of the mixture and $\widetilde{u_i}$ are the velocity vector coordinate.

Momentum Balance Equation

$$\frac{\partial\left(\overline{\rho}\tilde{u}_i\tilde{u}_j\right)}{\partial x_j} = \frac{\partial P'}{\partial x_j} + \frac{\partial\left(\tilde{\tau}_{ij}\right)}{\partial x_j}, \tag{10}$$

where the term $\tilde{\tau}_{ij}$ represents the Reynolds stress tensor and $\tilde{\tau}_{ij} = \mu_{eff}\left\{\left(\frac{\partial\tilde{u}_i}{\partial x_j} + \frac{\partial\tilde{u}_j}{\partial x_i}\right) - \frac{2}{3}\delta_{ij}\frac{\partial\tilde{u}_k}{\partial x_k}\right\}$. The effective viscosity is defined as $\mu_{eff} = \mu + \mu_T$, where μ_T is the eddy viscosity given by the turbulence model; $P' = \overline{P} + \frac{2}{3}\overline{\rho}k$ and P is the static pressure (gauge pressure); it is the difference between of the absolute pressure and operating pressure, $P_{abs} = P_0 + P_{gauge}$; k is the turbulent kinetic energy.

Total Energy Balance Equation

$$\frac{\partial\left(\tilde{u}_i\left(\overline{\rho}\tilde{h}\right)\right)}{\partial x_j} = \frac{\partial}{\partial x_j}\left(K_{eff}\frac{\partial\tilde{T}}{\partial x_j} - \sum_K h_K\tilde{J}_K\right) + S_h \tag{11}$$

where $\tilde{h}$ is the enthalpy of mixture, $\tilde{h} = \int_{T_{ref}}^{T} c_p dT$, with $T_{ref} = 273.15\,\mathrm{K}$. k_T is the turbulent thermal conductivity with $k_T = c_p\mu_T/\mathrm{Pr}_T$ and $\mathrm{Pr}_T = 0.85$ is the turbulent Prandtl number, $K_{eff} = k_m + k_T$ is the effective thermal conductivity and $\tilde{J}_k$ is the diffusive flux of the species. In this study, the energy variation due to the mixture enthalpy variation is accounted for in Eq. (11) by the source term S_h (Jerzy *et al*., 2004):

$$S_h = \overline{\rho}\widetilde{u_i}\left(\frac{\partial Q_m}{\partial Y_1}\widetilde{Y}_1 + Q_m\right)\frac{\partial\widetilde{Y}_1}{\partial x_i}. \tag{12}$$

The dependence of mixture heat Q_m with the concentration is calculated using the Peng-Robinson equation. S_h is inserted as part of the energy equation in a subroutine as a user defined function (UDF) (ANSYS, 2010).

Chemical Species Balance Equation

$$\frac{\partial}{\partial x_j}\left(\overline{\rho}\tilde{u}_j\widetilde{Y}_i\right) = -\frac{\partial}{\partial x_j}\left(\left(\overline{\rho}D_{eff}\right)\frac{\partial\widetilde{Y}_i}{\partial x_j} - D_{T,i}\frac{\nabla T}{T}\right), \tag{13}$$

where Y_i is mass fraction of the i^{ih} specie, $D_{eff} = D_{1,2} + D_T$, $D_{1,2}$ is the molecular diffusivity coefficient, $D_T = \frac{\mu_T}{Sc_T\overline{\rho}}$ is the turbulent diffusivity coefficient, Sc_T is the turbulent Schmidt number equal to 0.7. The turbulence model incorporates two differential transport equations into the resulting system of equations, one is for turbulent kinetic energy k and the other is for the dissipation rate of turbulent kinetic energy ε (Wilcox, 1993), for the k-ε turbulence model $\mu_T = \overline{\rho}k^2/\varepsilon$. In Eq. (13) $D_{T,i}$ is the thermal (Soret) diffusion coefficient of the i^{ih} specie.

Transport equation for the mixture fraction

$$\frac{\partial}{\partial x_j}\left(\overline{\rho}\tilde{u}_j\widetilde{f}_i\right) = -\frac{\partial}{\partial x_j}\left(\left(\overline{\rho}D_{eff}\right)\frac{\partial\widetilde{f}_i}{\partial x_j}\right), \tag{14}$$

In Eq. (14) f is the mixture fraction, which represents the mass fraction of fluid fed into the system from a chosen point (Fox, 2003) and is given by:

$$f = \frac{Y_{CO_2} - Y_{\alpha,CO_2}}{Y_{\alpha,sol} - Y_{\alpha,CO_2}}, \tag{15}$$

where Y_{α,CO_2} and $Y_{\alpha,sol}$ are the mass fractions of CO_2 in the CO_2 inlet and in the solvent inlet, respectively.

Mixture fraction variance, σ^2, can be understood as the deviation from the locally perfect mixture state, that is, the mixing process can be understood as the dissipation of such variance (Fox, 2003; Jerzy *et al*., 2004). The transport equations σ^2 are considered and inserted into the system of equations as user defined scalar –UDS - transport equations (ANSYS, 2010). Such equations are given, respectively, by:

Transport equation for the mixture fraction variance

$$\frac{\partial\left(\overline{\rho}\widetilde{u_i}\tilde{\sigma}^2\right)}{\partial x_i} = \frac{\partial}{\partial x_j}\left(\overline{\rho}\left(D_{eff}\right)\frac{\partial\tilde{\sigma}^2}{\partial x_j}\right) + \underbrace{2D_T\overline{\rho}\left(\frac{\partial\tilde{f}}{\partial x_j}\right)^2 - 2\overline{\rho}\frac{\tilde{\varepsilon}}{\tilde{k}}\tilde{\sigma}^2}_{S_\sigma}. \tag{16}$$

The term S_σ in Eq. (16) was entered via a subroutine as a UDF in the ANSYS FLUENT software.

The *k*-ε turbulence model transport differential equations based on turbulent viscosity are (Launder and Spalding, 1974):

Turbulent kinetic energy equation *k*

$$\frac{\partial\left(\rho k\tilde{u}_j\right)}{\partial x_j} = \frac{\partial}{\partial x_j}\left[\left(\mu + \frac{\mu_T}{\sigma_k}\right)\frac{\partial k}{\partial x_j}\right] + P_k - \rho\varepsilon \tag{17}$$

and

Dissipation rate of turbulent kinetic energy ε

$$\frac{\partial\left(\rho\varepsilon\tilde{u}_j\right)}{\partial x_j} = \frac{\partial}{\partial x_j}\left[\left(\mu + \frac{\mu_T}{\sigma_\varepsilon}\right)\frac{\partial\varepsilon}{\partial x_j}\right] + C_{\varepsilon 1}\frac{\varepsilon}{k}P_k - C_{\varepsilon 2}\rho\frac{\varepsilon^2}{k}. \tag{18}$$

In Eqs. (17 and (18) P_k is a production term of turbulence due to the viscous forces; the constants, $C_{\varepsilon 1} = 1.44$, $C_{\varepsilon 2} = 1.92$, $C_\mu = 0.09$, $\sigma_k = 1.0$, and $\sigma_\varepsilon = 1.3$ are closure constants found based on the correlation of experimental data. All mathematical derivations and the physical basis of the model can be found in detail in Rezende, R. V. d. P. (2008).

Operational Conditions and Boundary Conditions

Operational temperature values were considered in the range of 308 - 320 K. Operational pressure P_0 was tested at 80 bar and 120 bar per conditions displayed in Table 1. The values for density calculated using the Peng-Robinson equation employed in Eq. (8) of the diffusivity coefficient and the values calculated for pure component viscosities, using the Chung method for Eq. (6) of the mixture viscosity are also listed in Table 1.

Under all cases, inlet boundary conditions considered were operating temperature T_0 and mass flows rate: $1.1\text{x}10^{-4}$ kg/s for CO_2 and $1.2\text{x}10^{-5}$ kg/s for ethanol and the outlet boundary condition was considered to be zero pressure. Turbulence intensity was considered to be 5% (medium intensity) as the inlet and outlet boundary conditions.

Table 1: Operating conditions (T_0, P_0), density values, and viscosity values for the pure components**.**

Case	T_0 [K]	P_0 [bar]	ρ_{CO_2} [kg/m^3]	$\rho_{Ethanol}$ [kg/m^3]	μ_{CO_2} [Pa.s]	$\mu_{Ethanol}$ [Pa.s]
1	308.00	80.00	419.44	716.78	$3.51\text{x}10^{-5}$	$4.68\text{x}10^{-4}$
2	308.00	120.00	741.54	718.55	$5.35\text{x}10^{-5}$	$4.77\text{x}10^{-4}$
3	313.00	80.00	291.50	712.98	$2.94\text{x}10^{-5}$	$4.38\text{x}10^{-4}$
4	313.00	120.00	682.66	714.86	$4.896\text{x}10^{-5}$	$4.45\text{x}10^{-4}$
5	315.00	80.00	273.31	711.44	$2.86\text{x}10^{-5}$	$4.26\text{x}10^{-4}$
6	315.00	120.00	657.26	713.36	$4.72\text{x}10^{-5}$	$4.35\text{x}10^{-4}$
7	317.00	80.00	259.40	709.87	$2.81\text{x}10^{-5}$	$4.15\text{x}10^{-4}$
8	317.00	120.00	630.84	711.84	$4.56\text{x}10^{-5}$	$4.23\text{x}10^{-4}$
9	320.00	80.00	243.19	707.49	$2.753\text{x}10^{-5}$	$3.99\text{x}10^{-4}$
10	320.00	120.00	589.63	709.53	$4.43\text{x}10^{-5}$	$4.07\text{x}10^{-4}$

In order to initialize the equation system, a set of values was calculated based on the CO_2 inlet boundary conditions; these initial conditions favored the stabilization of the system of equations with respect to the other tested initializations conditions.

Numerical Methodology

The SAS chamber utilized consists of a cylindrical tank 120 mm long and 80 mm in diameter, taking into consideration the two-dimensional geometry as well as the axis symmetry, as outlined in Figure 1. The chamber is coupled with a coaxial capillary 20 mm long in the center of the lid with a central solvent inlet 0.01 mm in diameter and a CO_2 inlet measuring 0.1 mm in diameter. The outlet is in the center of the bottom of chamber and measures 3.45 mm in diameter.

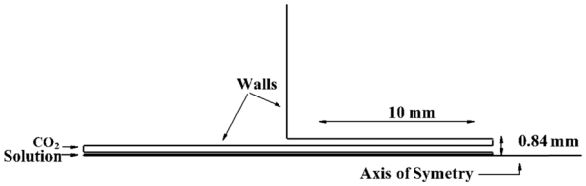

Figure 1: View of the geometry of the two-dimensional capillary tube used in the simulations of this work - with the axis of symmetry.

Based on the geometry and employing the ANSYS ICEM 13.0 software, a two-dimensional mesh composed of 115.5×10^3 hexahedral elements was generated after a mesh refinement study, because the jet development region is strongly influenced by mesh resolution. Thus, given that a greater refinement did not cause modifications in the field variables or in the jet shape. In Figure 2, one can visualize the details of the mesh refinement in the capillary output region.

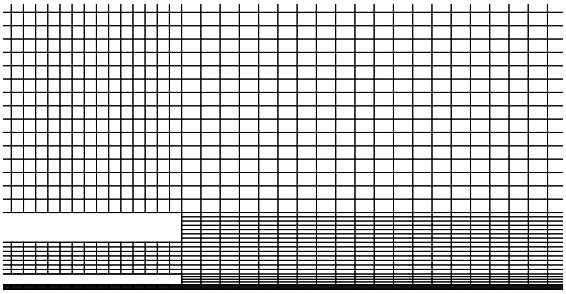

Figure 2: Detail of the hexahedral mesh refinement in the capillary region.

The finite volumes method was applied in order to solve the system of Equations (1)-(18), using the FLUENT 13.0 software. The segregated solver consisted of solving the resulting linear systems for each variable one at a time, updating their coefficients due to non-linearities and coupling among variables. The segregated solution scheme is shown in Figure 3.

The SIMPLE algorithm was used to solve the pressure-velocity coupling. Because convergence criteria were imposed, a Root Mean Square residue (RMS) of less than 10^{-5} for all the variables and closure for mass balance was observed, *i.e*, the differences between the inlet and outlet mass flow rates were of the order of $|10^{-11}|$.

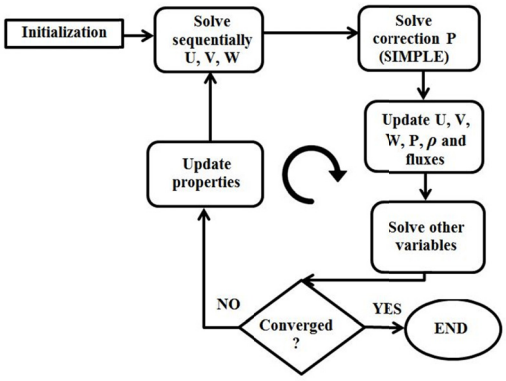

Figure 3: Solution scheme employed by the segregated solver (ANSYS, 2010)

The solution proved convergence to be difficult and presented instability upon simultaneously solving the complete system of equations. It was possible to obtain convergence of the solution upon sequentially adding equations in the following manner (Almeida, 2013):

Step 1 - once convergence of the continuity and momentum equations is reachead, activate the species transport equations;

Step 2 - if converged, activate the energy equation;

Step 3 - once these fields present convergence, activate the equations involving the other variables (mixture fraction, mixture fraction variance).

RESULTS AND DISCUSSION

Density Dependence on Temperature and Pressure Differentials

The Peng-Robinson cubic flow equation (Equations (1)-(5)) was employed in order to predict how

sensitive the density of the mixture ρ is to differential variations in pressure and temperature surrounding its operational values T_0 = 313 K and P_0 = 120 bar. Considering that:

$$d\rho = \left(\frac{\partial \rho}{\partial P}\right)_T dP + \left(\frac{\partial \rho}{\partial T}\right)_P dT, \tag{19}$$

and the Taylor series expansion of ρ:

$$\rho\left(P_0 + dP, T_0 + dT, Y_i^0\right) = \rho(P_0, T_0, Y_i^0) + dP\left(\frac{\partial \rho}{\partial P}\right)_T + dT\left(\frac{\partial \rho}{\partial T}\right)_P + o\left(dP^2, dT^2\right). \tag{20}$$

Substituting Eq. (19) into Eq. (20), neglecting the second order and higher order terms in Eq.(20), the result can be writen as:

$$\rho\left(P_0 + dP, T_0 + dT, Y_i^0\right) \cong \rho(P_0, T_0, Y_i^0) + d\rho. \tag{21}$$

Maintaining $Y_1^0 = 0.1$, one observes that, if the temperature varies dT = ± 7 K within the SAS chamber, the density differential would subsequently vary ± 30 kg/m^3. On the other hand, if the pressure varies dP = ± 7 bar, it would produce a density differential of ± 8.8 kg/m^3, as shown in Figure 4 (a) and (b)), respectively. As such, 7 K represents 2.2% of operational temperature (T_0 = 313 K) and causes a density variation three times greater than the pressure differential of 7 bar, which itself represents 5.8% of the operational pressure (P_0 = 120 bar). Thus, given Eq. (21), knowing $\rho(P_0, T_0, y_i^0)$, the density is much more sensitive to temperature change within the chamber than to comparable alterations in pressure.

This assertion remains consistent for compositions of $Y_1^0 \leq 0.4$ and operational conditions within the range of T_0 (280 - 325 K) and P_0 (70 bar - 220 bar). At lower operational temperatures, the incremental contribution of pressure to the mixture density is still smaller than three times the temperature's incremental contribution.

Thus, if the condition for precipitation of a detemined solute were T_0 < 325 K, even with a high operational pressure requirement (70 - 220 bar), the temperature variation within the chamber is more determinant of mixture density than pressure variation.

Jet Dinamics

Opening Angle of the Jet: Model Verification

In order to validate and verify the model, the aperture angle of the jet formed at the outlet of the coaxial capillary obtained in this study was compared to that predicted in literature. A jet interacts with the surrounding fluid, dragging the fluid in which it is injected towards its own center and, in so doing, increases its mass flux. This process is known as entrainment. The boundary of the jet becomes delimited and, within this region, the fresh solvent entering the chamber brings surrounding CO_2. This is the portion of the chamber in which there is the greatest probability for particle nucleation (Petit-Gas *et al.*, 2009) due to the appearance of compositional non-homogeneities.

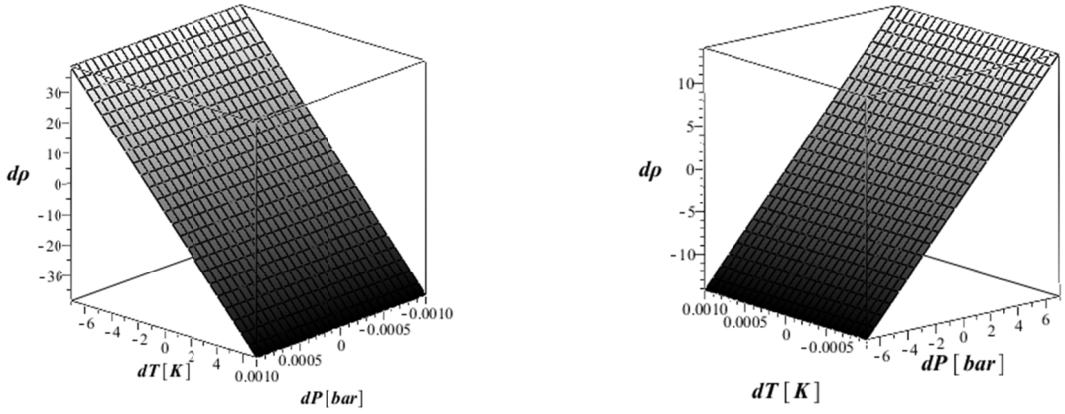

(a) (b)

Figure 4: Variation of $d\rho$ [kg/m^3] for mass fraction of ethanol with Y_1 = 0.1: (a) With incremental temperature variations of ± 7 K. (b) With incremental pressure variations of ± 7 bar.

From entrainment theory, the analytical solution for turbulent jets foresees an aperture of 11.8° (degrees) for circular nozzles. The Gaussian velocity profile follows that described by Cushman-Roisin (2013). In the cases considered here, the boundary of the jet was defined based on the velocity profiles in Figure 5 and the aperture angle was then obtained. The aperture angle obtained for each condition in Table 1 was approximately 12°. The Gaussian velocity profile of the jet was also observed, as shown in Figure 5. Regarding the velocity of the jet, with increasing pressure there was a decrease in the magnitude of the velocity and, with the increase of temperature, there was an increase in velocity. These facts have been observed by (Reitz Cardoso *et al*., 2013).

Influence of Pressure and Temperature the Patterns of the Solvent Jet

This study found that there is a gradual increase in the length and in the width of the jet of ethanol, *i.e*., a small increase amount of ethanol in the outlet of the capillary tube with an increase of the operational pressure (Figure 6); the greatest increase in length of the jet of solvent (observed under the pressure of 120 bar) was obtained with T_0 = 320 K.

Temperature Variations

Variations of energy in the form of heat were taken into consideration during the precipitation process through the mixture heat source term associated with the energy equation balance. When this term was not employed, the chamber temperature suffered a variation of approximately 1.4 K at the capillary tube exit in all the simulated cases. When this term was inserted into the energy equation under pressure at P_0 = 80 bar, there was an average reduction in T of 5 K in the chamber immediately after the capillary tube exit, as can be seen in Figure 7 and Figure 8 (a).

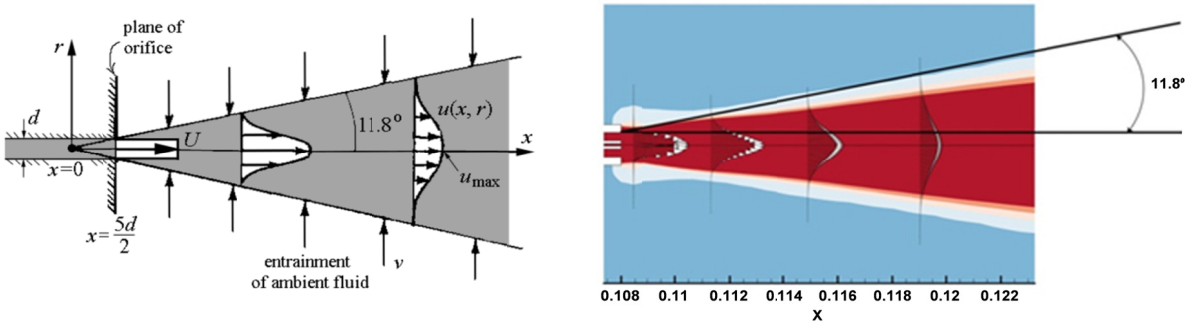

Figure 5: Comparison between the solution jet aperture as described in the literature (Cushman-Roisin, 2013) and that obtained though this study at 80 bar and 313 K.

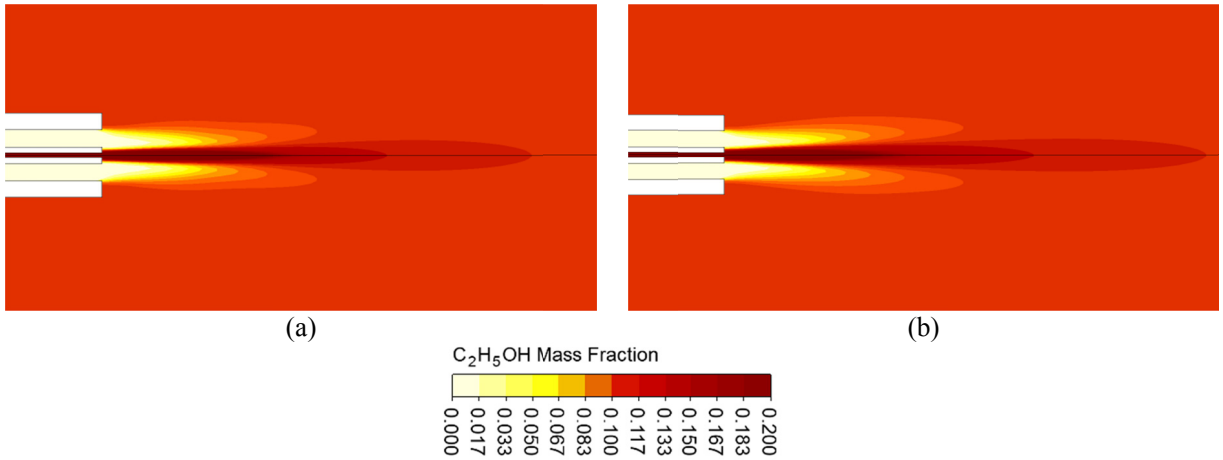

Figure 6: Influence of pressure on the solvent jet length at T_0 = 320 K. (a) P_0=80 bar; (b) P_0=120 bar. With higher pressure there is a more deep penetration of the fluid stream into the chamber.

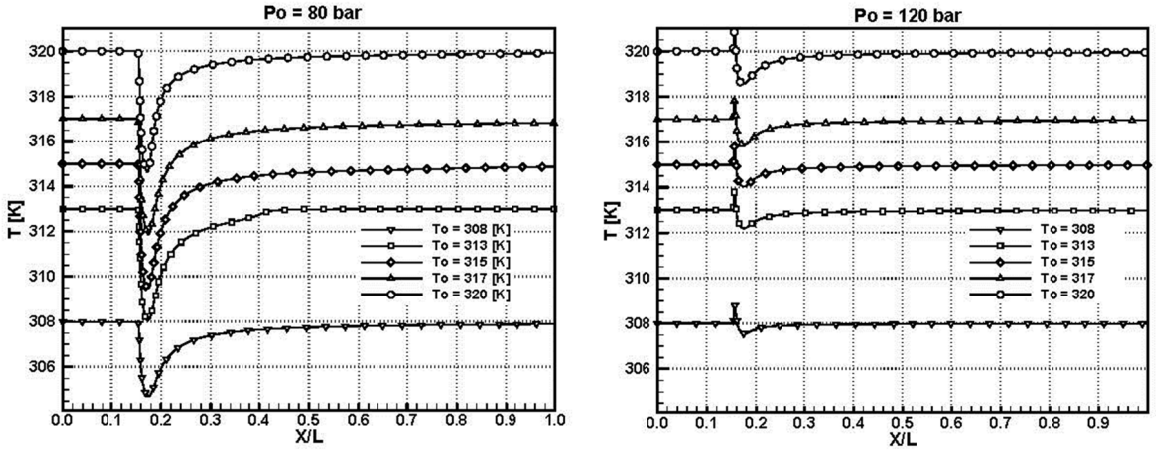

Figure 7: Temperature variation through the central axial line of the chamber at $P_0 = 80$ bar (end of the capillary X/L ~ 0.15).

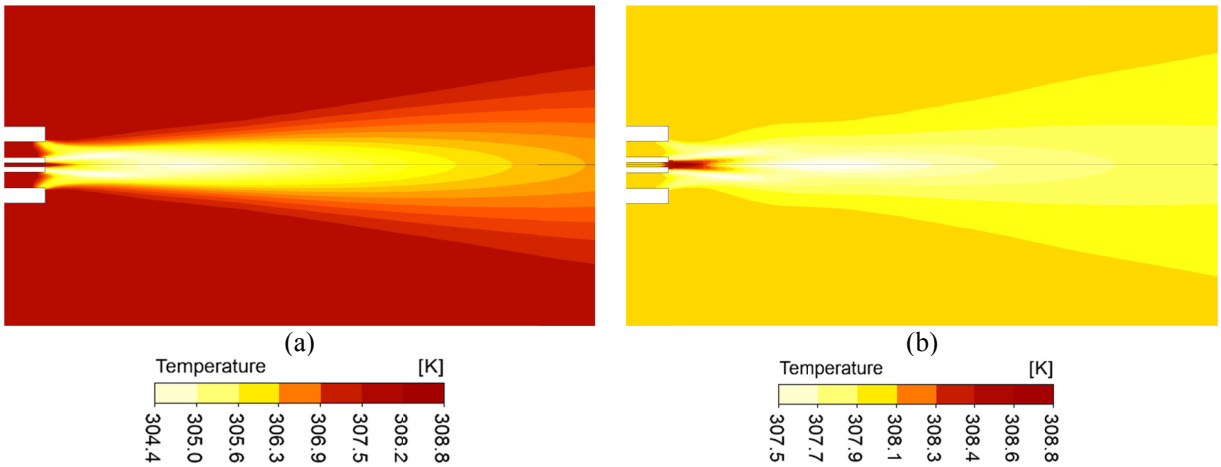

Figure 8: Temperature variation at the end of the capillary: (a) $T_0 = 308$ K $P_0 = 80$ bar; (b) $T_0 = 308$ K $P_0 = 120$ bar.

When the pressure is set to $P_0 = 120$ bar, initially there is a temperature increase of approximately 1 K above T_0 immediately following the capillary tube exit, with a subsequent 1 K fall below T_0, as can be seen in Figure 8 and Figure 9 (b).

Thus, there is greater temperature variation when operating the process at lower pressure. In both cases, after the mixture region located at the capillary exit, a homogenization of the temperature field is observed, which remains constant at a level of approximately T_0 value within the remainder of the chamber. These temperature variations, though relatively small, may significantly interfere with the density field, as observed in the previous section, and may inteferer in the precipitation mechanisms, since the variations occur within the entraining region of the CO_2 in the solvent jet, which is the most probable nucleation region and temperature is one of the variables that govern the rate of nucleation (Mullin, 2001).

Figures 8 (a) and (b) show the temperature variations at the end of the capillary tube. In this region for the two pressures conditions tested there are areas of cooling out of the center line of the chamber, near the border of the jet. According to Mullin (2001), the nucleation rate is inversely proportional to the rate of nucleation.

Pressure Variations

Under both operational pressure conditions considered, P_0 = 80 bar and P_0 = 120 bar, the decrease in pressure was approximately 0.9 bar in all cases simulated. This variation occurred inside the injection capillary, as shown in Figure 9. Within the interior of the chamber, no pressure variations were recorded.

The greatest presure variation inside the capillary tube under both operational pressure conditions occurred at the lower temperature studied, T_0 = 308 K. Pressure variations within the SAS camera have not been well studied or related to the process of nucleation and growth of particles in the literature.

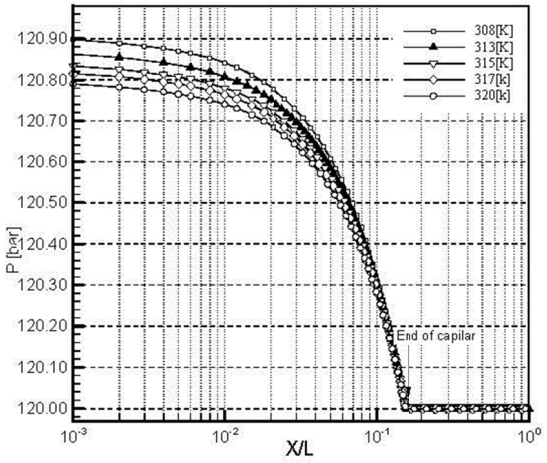

Figure 9: Pressure decreases on the central axis within the chamber at P_0 = 120 bar.

Density Variation

Precipitation employing supercritical fluid involves a thermodynamic equilibrium problem. A supercritical state mixture is a non-homogeneous environment with regions of high and low densities. When a solution containing a solute and a solvent is immersed within this environment, the average density of the solvent within the region around a molecule of solute differs from the density of the surrounding CO_2 (Braeuer *et al*., 2011).

For lower pressure, the CO_2 density is lower (as shown in Figure 10 in the external part of the capillary); this decreases the solubility in the organic solvent resulting in slower mass transfer, slow rates of nucleation and hence larger particles (Kim and Shing, 2008). If the difference in density between pure solvent and pure CO_2 is small, the average lifetime of a droplet is short and there is a small maximum droplet radius (Werling and Debenedetti, 2000). For the conditions under study here, the region with the smallest density difference within the chamber occurred at P_0=120 bar at the capillary exit (which are observed approximately 6 mm ahead of the capillary exit) as shown the comparison in Figure 10 for P_0=80 bar and P_0=120 bar (note that within this region the greatest temperature variation was also observed, as shown in Figure 8). Figure 10 also delimited the boundary of the jet (region highlighted with black lines), where there is the greatest probability of nucleation occurrence (De Marco and Reverchon, 2011; Lengsfeld *et al*., 2000).

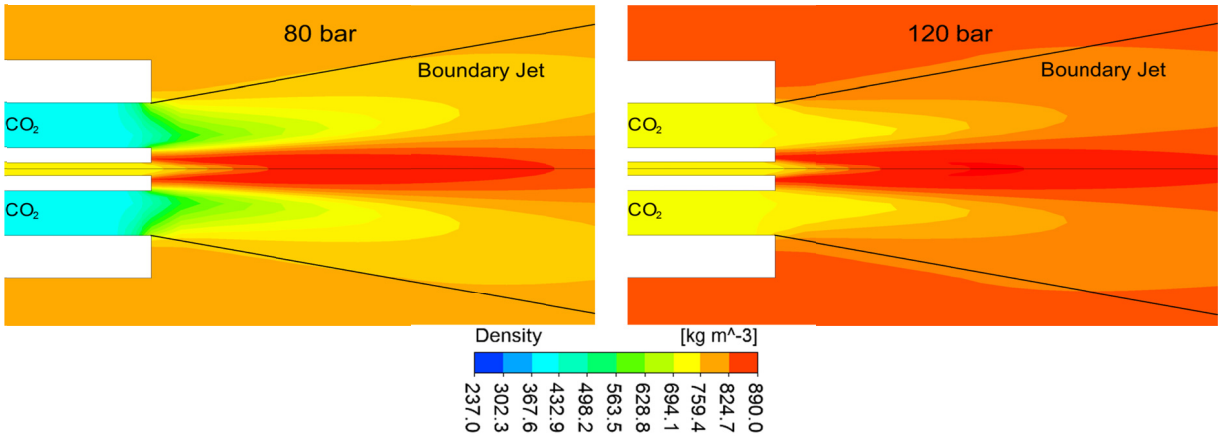

Figure 10: Density distribution in the capillary exit for the two considered operating pressures and the operating temperature of 308 K.

With an increase in temperature T_0, the mixture density reduces in the interior of the chamber, as indicated in graphs at the center line of the chamber in Figure 11. In this case, when P_0 was at 120 bar, the density of the mixture was highest due to increased T_0.

Physical Properties: Viscosity, Thermal Conductivity and Diffusivity

Viscosity, thermal conductivity, and the diffusivity coefficient of the supercritical mixture were evaluated. These three properties presented variation, but only in the small region of the capillary injection exit (1.5 mm length), remaining practically constant throughout the remainder of the interior of the precipitation chamber.

Viscosity

According to Chung's rule, molecular viscosity variation, through the central line of the chamber for the temperatures T_0 analyzed and pressures P_0 = 80 bar and P_0 = 120 bar can be seen in the graph in Figure 12. There is an abrupt drop in viscosity at the capillary tip (located at X/L = 0.15) which stabilizes at X/L = 0.21 and stays constant throughout the remainder of the length of the chamber. Increasing T_0 results in diminished viscosity levels.

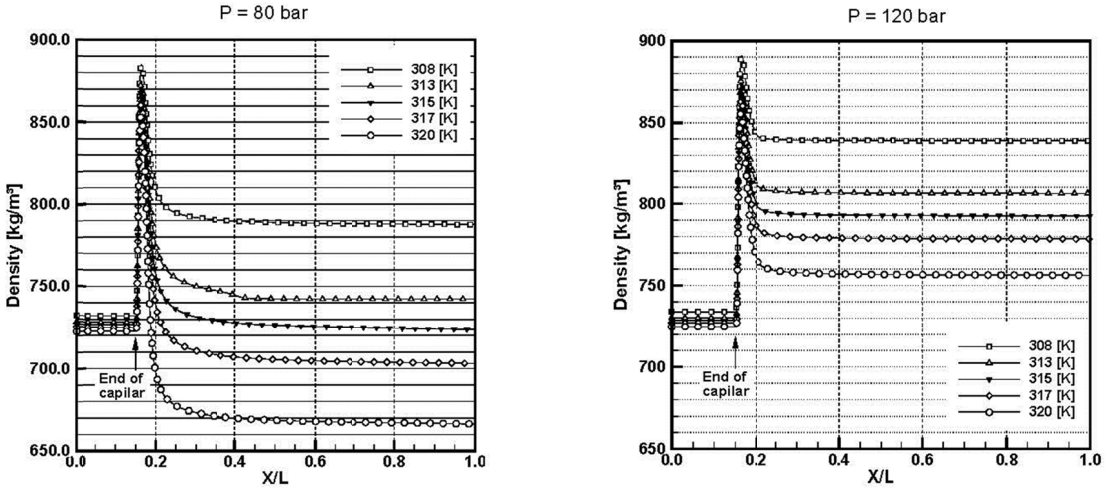

Figure 11: Density of the mixture through the center line of the chamber, at P_0 = 80 bar and P_0=120 bar.

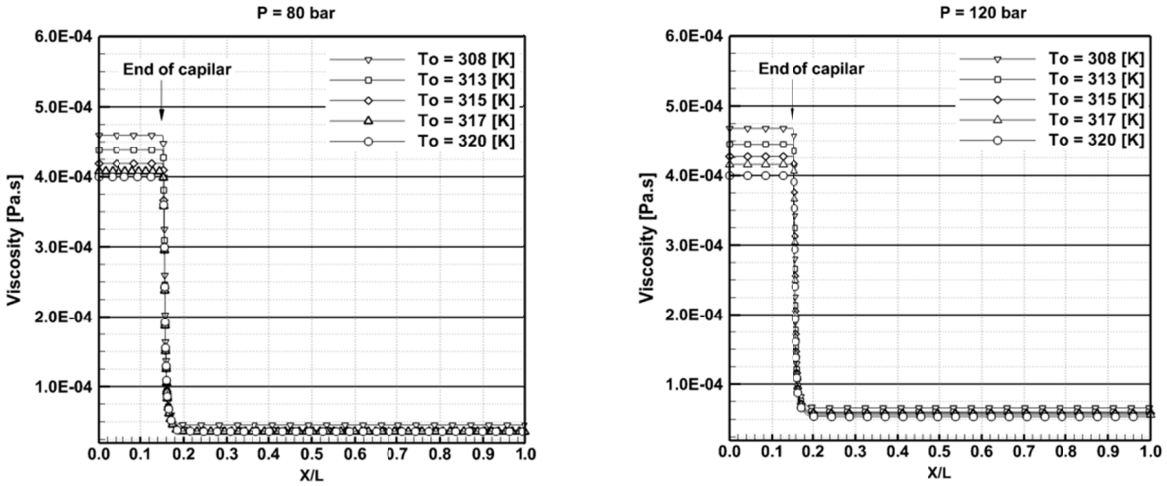

Figure 12: Viscosity of the mixture through the central line of the SAS chamber at P_0 = 80 bar and P_0 = 120 bar.

From Figure 12 under the operating pressure of 80 bar, the viscosity showed a small decrease compared with P_0 = 120 bar. From Figure 11 a large variation in the density of the mixture is observed with the variation of P_0. These facts confirm the conjecture made by Erriguible *et al*. (2013b) that, in supercritical conditions, increasing the operating pressure results in moderate impacts upon viscosity and significant impacts upon mixture density.

Diffusivity Coefficient

The diffusivity coefficient, according to Riazi-Whitson's equation, increases with the operational temperature. Its variation along the central axial line of the chamber interior due to operational temperature can be seen in the graph of Figure 13. For all cases simulated, upon increasing the operational pressure from 80 to 120 bar, there is a very small reduction in the magnitude of the diffusivity coefficient.

Thermal Conductivity

Thermal conductivity, according to Chung's rule, presented little variation with respect to temperature inside the chamber for an operational pressure of 80 bar. At the pressure of P_0 = 120 bar, greater values of λ occur in the injection capillary, namely 1.02 W/K.m at T_0 = 320 K and 1.22 W/K.m at T_0 = 308 K. It suffered an abrupt decrease of approximately 0.22 W/K.m just in front of the injection capillary exit under all temperature conditions and was constant throughout the remainder of the chamber interior, as detailed in Figure 14.

Turbulent Properties of the Mixture

The *k-ε* turbulence model was employed to take into account the effects of turbulence on the results obtained with the mathematical model presented. Analyses of field variables: eddy viscosity ratio, thermal conductivity ratio and diffusion coefficient ratio, were performed. These variables are the ratio between the turbulent and molecular contributions, i.e., $D_T/D_{1,2}$ μ_T/μ_m , k_T/k_m respectively. The results showed that, for the cases of Table 1 under the conditions analyzed in this study, the molecular properties contributions are important only on region near the chamber walls, except the thermal conductivity, for which the molecular contribution in the chamber is also dominant in the initial region of the jet boundary, as shown in Figure 15. Thus, for the region of interest for precipitation (at the exit of the capillary tube and on the border of the jet) the contributions of molecular viscosity and the coefficient of molecular diffusivity are negligible and the mass transport is due to turbulence.

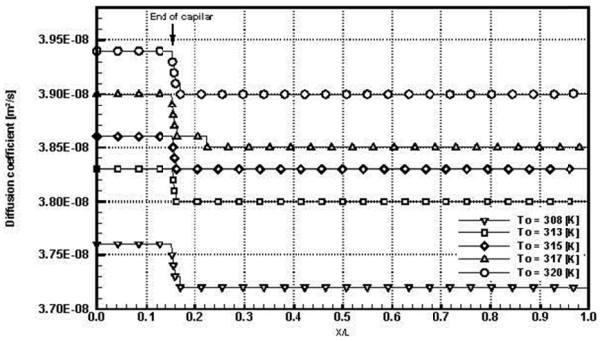

Figure 13: Diffusivity coefficient of the mixture through the central axial line of the SAS chamber at P_0 = 120 bar (end of X/L ~ 0.15).

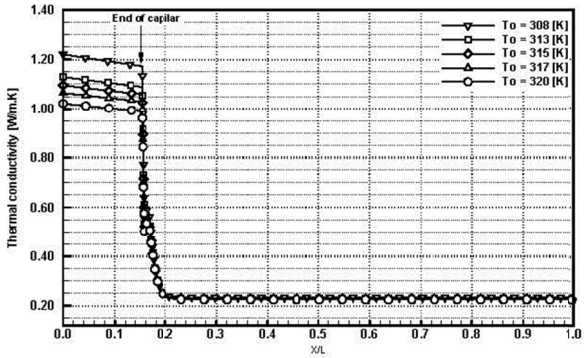

Figure 14: Thermal conductivity along the central axial line of the chamber at P_0 = 120 bar (capillary tip X/L ~ 0.15).

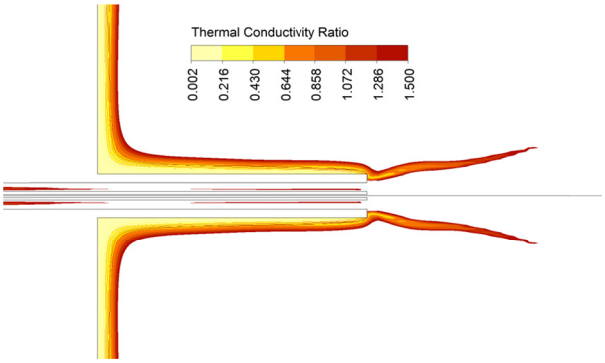

Figure 15: Contours for the thermal conductivity ratio in outlet of the capilar region where $k_T/k_m < 1$ for T_0=313 K and P_0=120 bar.

However, other studies using different models of turbulence and sensitivity analyses of the molecular properties (μ_m, $D_{1,2}$ and k_m) with incrementals of T and P can be made in order to reevaluate the effect of T_0, P_0 and of turbulence on the SAS process.

FLOW DYNAMICS: MIXTURE

In supercritical conditions, the formation of a homogenous mixture between the solvent and the antisolvent at a molecular level is the most important question to be determined in order to acheive nucleation and approximately spherical nanometric particle growth (Fox, 2003). The intensity of segregation is given by:

$$I_s = \tilde{\sigma}^2 \Big/ \tilde{f}\left(1-\tilde{f}\right), \tag{22}$$

In Eq. (22), I_s is equal to unity when the fluid elements are not mixed well on a molecular scale and is equal to zero when the molecular scale mixture is perfect (Henczka *et al.*, 2005). In this work, I_s is calculated in the post-processing stage in ANSYS CFD-Post 13.0, when the variables σ^2 and $\tilde{f}$ are known, assuming a clip range of $0.0001 \leq \tilde{f} \leq 0.9999$, because I_s become singular when $\tilde{f} \in \{0, 1\}$. For all simulated conditions, the intensity of segregation approaches zero in practically on the entire interior of the chamber. Only at the capillary tube exit is there a significant increase in the magnitude of this variable, because it is the place where the mixing process begins (where the fluids are not yet well mixed and the mixture is poor). After this region, one can affirm that the mixture is perfect on a molecular scale.

Given the pressure condition $P_0 = 80$ bar, the intensity of segregation values also remains close to zero. However, they are slightly higher than those observed for the pressure $P_0 = 120$ bar, as can be seen in Figure 16. This indicates that the tendency for the best mixture is observed at higher operational pressure. Hence, there is more efficient mixing at the molecular scale for higher operating pressure, corroborating the experimental observation of the literature that, under higher pressure, smaller particle sizes are observed (Boschetto, 2013; Franceschi, 2009; Reverchon and De Marco, 2011).

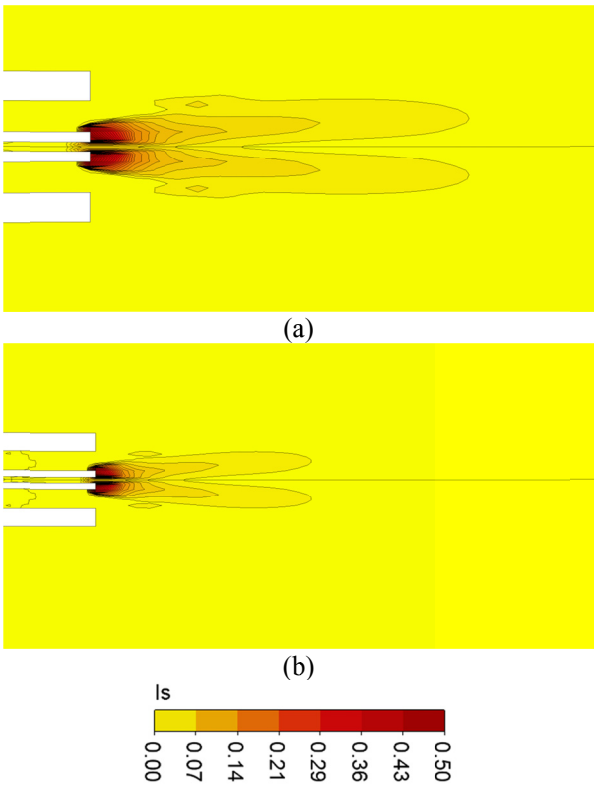

Figure 16: Intensity of segregation at the capillary injection exit region at T_0=308 K. (a) At P_0=80 bar; (b) At P_0=120 bar, in which higher *Is* values are observed.

CONCLUSION

In this study, a mathematical model to describe the flow of a supercritical CO_2 and ethanol mixture in non-isothermal, compressible turbulent and permanent regime was employed to evaluate the effect of operating temperature and the operating pressure on the properties: density, viscosity, thermal conductivity and diffusivity. In so doing, this study also presents the effect of operating temperature and the operating pressure upon the dynamics of the mixture in the SAS process.

There is an almost constant pressure variation within the precipitation chamber, namely, its variation is restricted to the injection capillary. Pressure changes influence much less the mixture density than the respective temperature variations. Thus, a consideration of mixture density formulation that depends exclusively upon temperature and of the mixture composition is a good numerical strategy towards

more effective SAS chamber modeling, deminishing both computational time and computational effort.

Regarding the jet boundary, the results were corroborated with analytical outputs comparing with the opening angle and the gaussian velocity profile given in the relevant literature. In all, these indicate the appropriate formulation of the proposed model.

When the heat of mixture term is added in the energy equation, the temperature distribution undergoes a greater variation (about 5 K) when the lowest operational pressure is considered. The greatest variations of composition, temperature, and physical properties under consideration occurred within a small region that begins at the capillary exit.

The physical properties μ_m, k_m, and $D_{1,2}$, dependent upon T, P, and Y_i, were considered. Turbulent properties dominate the molecular properties in the process. With the turbulence model employed under the conditions considered, it was concluded that, in this case, it is possible to use less complex equations than Equations (7), (8) and (9) in the model, reducing the computational time, except for the thermal conductivity under an operating pressure of 120 bar. Within the SAS chamber, based on the variable intensity of segregation, a good molecular scale mixture was observed for all conditions simulated, mainly at the higher operating pressure.

The model presented herein offers ease and speed in obtaining results using only a desktop computer, reducing the time and cost of laboratory experiments. The next steps of this work will be to apply the 3D approach, as well as a study on a larger scale of operational conditions with variation of the inlet flow rate of CO_2 and the inlet flow rate of solvent, and improve understanding of the effects of turbulence on the mixture process, as well as coupling with a model to predict the dynamics of particle growth. In so doing, greater understanding is to be gained concerning the precipitation mechanisms, experimental costs will significantly reduced, and the SAS process become more efficient.

ACKNOWLEDGEMENTS

The authors would like to thank the Coordination for Improvement of Higher Education Personnel-CAPES (www.capes.gov.br) for granting financial support to the first author, enabling the development of this work.

NOMENCLATURE

c_v	Heat capacity at constant volume [J mol^{-1}K^{-1}]
$D_{1,2}$	Molecular diffusion coefficient of the mixture [m^2/s]
D^0	Diffusion coefficient at low pressure [cm^2/s]
k_m	Thermal conductivity of the mixture [$W\ m^{-1}K^{-1}$]
k	Turbulent kinetic energy [m^2 s^{-2}]
M	Molecular weight of the mixture [kg/mol]
$\dot{m}_{CO_2}$	Mass flow rate of CO_2 [kg s^{-1}]
$\dot{m}_{sol}$	Mass flow rate of Solvent [kg s^{-1}]
P	Pressure [bar]
P_0	Operational Pressure [bar]
P_{cm}	Critical Pressure of the mixture [bar]
P_{ci}	Critical Pressure of component *i* [bar]
Pc_m	Critical mixture Pressure [bar]
R	Universal constant for gases [J mol^{-1}.K^{-1}]
Re	Reynolds number
T	Temperature [K]
T_{cm}	Critical Temperature of the mixture [K]
T_{ci}	Critical Temperature of component *i* [K]
T_0	Operational Temperature [K]
Tri	Reference Temperature of component *i*
Tr_m	Reduced Temperature of the mixture
V	Molar volume [m^3 mol^{-1}]
V_{cm}	Critical volume of the mixture [cm^3 mol^{-1}]

Greek Symbols

ε	Turbulent kinetic energy rate of dissipation [m^{2}s^{-3}]
μ_m	Dynamic viscosity of the mixture [Pa.s]
ρ	Mixutre density [kg m^{-3}]
ω_m	Acentric factor of the mixture

REFERENCES

Almeida, R. A., Study of turbulent flow in capillary supercritical fluid applied to the production of nanoparticles. (PhD thesis), State University of Maringa, Brazil (2013).

ANSYS, F. ANSYS Fluent, Inc. User Guide. Retrieved from http://www.ansys.com (2010).

Balcão, V. M., Costa, C. I., Matos, C. M., Moutinho, C. G., Amorim, M., Pintado, M. E., Gomes, A. P., Vila, M. M., Teixeira, J. A., Nanoencapsulation of bovine lactoferrin for food and biopharmaceutical

applications. Food Hydrocolloids, 32(2), 425-431 (2013). doi: http://dx.doi.org/10.1016/j.foodhyd.2013.02.004

Bałdyga, J., Kubicki, D., Shekunov, B. Y., Smith, K. B., Mixing effects on particle formation in supercritical fluids. Chemical Engineering Research and Design, 88(9), 1131-1141 (2010). doi: http://dx.doi.org/10.1016/j.cherd.2010.02.016

Boschetto, D. L., Encapsulamente De Extrato de Semente de Uva, Astaxantina e Bixina Utilizando a Técnica SEDS. (Doutor em Engenharia de Alimentos), Universidade Federal de Santa Catarina, Florianópolis, SC (2013). (In Portuguese).

Braeuer, A., Adami, R., Dowy, S., Rossmann, M., Leipertz, A., Observation of liquid solution volume expansion during particle precipitation in the supercritical CO_2 antisolvent process. The Journal of Supercritical Fluids, 56(2), 121-124 (2011). doi: http://dx.doi.org/10.1016/j.supflu.2010.12.015

Cardoso, M. A. T., Cabral, J. M. S., Palavra, A. M. F., Geraldes, V., CFD analysis of supercritical antisolvent (SAS) micronization of minocycline hydrochloride. The Journal of Supercritical Fluids, 47(2), 247-258 (2008). doi: http://dx.doi.org/10.1016/j.supflu.2008.08.008

Chang, S.-C., Lee, M.-J., Lin, H.-M., Role of phase behavior in micronization of lysozyme via a supercritical anti-solvent process. Chemical Engineering Journal, 139(2), 416-425 (2008). doi: http://dx.doi.org/10.1016/j.cej.2007.12.008

Chung, T. H., Ajlan, M., Lee, L. L., Starling, K. E., Generalized multiparameter correlation for nonpolar and polar fluid transport properties. Industrial & Engineering Chemistry Research, 27(4), 671-679 (1988). doi: 10.1021/ie00076a024

Cushen, M., Kerry, J., Morris, M., Cruz-Romero, M., Cummins, E., Nanotechnologies in the food industry – Recent developments, risks and regulation. Trends in Food Science & Technology, 24(1), 30-46 (2012). doi: http://dx.doi.org/10.1016/j.tifs.2011.10.006

Cushman-Roisin, B., Environmental Fluid Mechanics. United States of America: John Wiley & Sons, Inc. (2013).

De Marco, I., Reverchon, E., Influence of pressure, temperature and concentration on the mechanisms of particle precipitation in supercritical antisolvent micronization. The Journal of Supercritical Fluids, 58(2), 295-302 (2011). doi: http://dx.doi.org/10.1016/j.supflu.2011.06.005

Erriguible, A., Fadli, T., Subra-Paternault, P., A complete 3D simulation of a crystallization process induced by supercritical CO_2 to predict particle size. Computers & Chemical Engineering, 52 (0), 1-9 (2013a). doi:http:// dx.doi.org/10.1016/j.compchemeng.2012.12.002

Erriguible, A., Laugier, S., Laté, M., Subra-Paternault, P., Effect of pressure and non-isothermal injection on re-crystallization by CO_2 antisolvent: Solubility measurements, simulation of mixing and experiments. The Journal of Supercritical Fluids, 76(0), 115-125 (2013b). doi: http://dx. doi.org/10.1016/j.supflu.2013.01.015

Fox, R. O., Computational Models for Turbulent Reacting Flows. United States of America: Cambridge University Press, New York (2003).

Franceschi, E., Precipitação e Encapsulamento de beta-Caroteno em PHBV Empregando Tecnologia Supercrítica. (Grau de Doutor), Universidade Federal de Santa Catarina, Florianópolis-SC (2009). (In Portuguese).

Franceschi, E., De Cesaro, A. M., Feiten, M., Ferreira, S. R. S., Dariva, C., Kunita, M. H., Rubira, A. F., Muniz, E. C., Corazza, M. L., Oliveira, J. V., Precipitation of β-carotene and PHBV and co-precipitation from SEDS technique using supercritical CO_2. The Journal of Supercritical Fluids, 47(2), 259-269 (2008). doi: http://dx.doi.org/10.1016/j.supflu.2008.08.002

He, C.-H., Yu, Y.-S., New equation for infinite-dilution diffusion coefficients in supercritical and high-temperature liquid solvents. Industrial & Engineering Chemistry Research, 37(9), 3793-3798 (1998). doi: 10.1021/ie970898+

Henczka, M., Bałdyga, J., Shekunov, B. Y., Particle formation by turbulent mixing with supercritical antisolvent. Chemical Engineering Science, 60, 2193- 2201 (2005).

Imsanguan, P., Pongamphai, S., Douglas, S., Teppaitoon, W., Douglas, P. L., Supercritical antisolvent precipitation of andrographolide from *Andrographis paniculata* extracts: Effect of pressure, temperature and CO_2 flow rate. Powder Technology, 200(3), 246-253 (2010). doi: http://dx.doi.org/10.1016/j.powtec.2010.02.031

Jerzy, Boris, S., Marek, H., Baldyga, Fluid Dynamics, Mass Transfer, and Particle Formation in Fluids. Supercritical Fluid Technology for Drug Product Development: Informa Healthcare (2004).

Kim, Y. H., Shing, K. S., Supercritical fluid-micronized ipratropium bromide for pulmonary drug delivery. Powder Technology, 182(1), 25-32 (2008). doi: http://dx.doi.org/10.1016/j.powtec.2007.04.009

Launder, B. E., Spalding, D. B., The numerical computation of turbulent flows. Computer Methods in Applied Mechanics and Engineering, 3, 20 (1974).

Lengsfeld, C. S., Delplanque, J. P., Barocas, V. H., Randolph, T. W., Mechanism governing micro-

particle morphology during precipitation by a compressed antisolvent: Atomization vs nucleation and growth. The Journal of Physical Chemistry, B, 104 (12), 2725-2735 (2000). doi: 10.1021/ jp9931511

Martín, A., Cocero, M. J., Numerical modeling of jet hydrodynamics, mass transfer, and crystallization kinetics in the supercritical antisolvent (SAS) process. The Journal of Supercritical Fluids, 32(1-3), 203-219 (2004). doi: http://dx.doi.org/10.1016/ j.supflu.2004.02.009

Martín, A., Cocero, M. J., Micronization processes with supercritical fluids: Fundamentals and mechanisms. Advanced Drug Delivery Reviews, 60(3), 339-350 (2008). doi: http://dx.doi.org/10.1016/j. addr.2007.06.019

Martín, A., Mattea, F., Gutiérrez, L., Miguel, F., Cocero, M. J., Co-precipitation of carotenoids and bio-polymers with the supercritical anti-solvent process. The Journal of Supercritical Fluids, 41(1), 138-147 (2007). doi: http://dx.doi.org/10. 1016/j.supflu.2006.08.009

Miguel, F., Martín, A., Gamse, T., Cocero, M. J., Supercritical anti solvent precipitation of lycopene: Effect of the operating parameters. The Journal of Supercritical Fluids, 36(3), 225-235 (2006). doi: http://dx.doi.org/10.1016/j.supflu.2005. 06.009

Mullin, J. W., Crystallization. (Fourth Ed.). University of London, Butterworth-Heinemann (2001).

Petit-Gas, T., Boutin, O., Raspo, I., Badens, E., Role of hidrodynamics in supercritical antisolvent process. The Journal of Supercritical Fluids, 7 (2009).

Poling, B. E., Prausnitz, J. M., O'Connell, J. P., The Properties of Gases and Liquids. McGraw-Hill Companies (2004).

Raffel, M., Willert, C. E., Kompenhans Jr., Particle Image Velocimetry: A Practical Guide. Berlin, New York, Springer (1998).

Reitz Cardoso, F. A., Almeida, R. A., Rezende, R. V. P., Cardozo-Filho, L., Noriler, D., Meier, H. F., Cabral, V. F., Influence of Pressure and Temperature on the Velocity of a Turbulent Jet Flow 3D. David Publishing, 8, 8 (2013).

Reverchon, E., Adami, R., Caputo, G., De Marco, I., Spherical microparticles production by supercritical antisolvent precipitation: Interpretation of results. The Journal of Supercritical Fluids, 47(1), 70-84 (2008). doi: http://dx.doi.org/10.1016/ j.supflu. 2008.06.002

Reverchon, E., De Marco, I., Mechanisms controlling supercritical antisolvent precipitate morphology. Chemical Engineering Journal, 169(1-3), 358-370 (2011). doi: http://dx.doi.org/10.1016/j. cej.2011.02. 064

Reverchon, E., De Marco, I., Torino, E., Nanoparticles production by supercritical antisolvent precipitation: A general interpretation. The Journal of Supercritical Fluids, 43(1), 126-138 (2007). doi: http://dx.doi.org/10.1016/j.supflu.2007.04.013

Reverchon, E., Torino, E., Dowy, S., Braeuer, A., Leipertz, A., Interactions of phase equilibria, jet fluid dynamics and mass transfer during supercritical antisolvent micronization. Chemical Engineering Journal, 156(2), 446-458 (2010). doi: http://dx.doi.org/10.1016/j.cej.2009.10.052

Rezende, R. V. P., Modelagem Matemática e Desenvolvimento de Metodologia Computacional Para a Simulação Numérica do Escoamento Bifásico de Ar e Ferro-Gusa em Canal de Corrida de Alto-Forno. (Dissertação de Mestrado), Universidade Federal de Santa Catarina, Florianópolis-SC (2008). (In Portuguese).

Rezende, R. V. P., Oshiro, H. K., Velocimetria Laser. Relatório Técnico Rede de Fluido Dinâmica Computacional-UFSC (2010). (In Portuguese).

Riazi, M. R., Whitson, C. H., Estimating diffusion coefficients of dense fluids. Ind. Eng. Chem. Res., 3081-3088 (1993).

Sanguansri, P., Augustin, M. A., Nanoscale materials development – a food industry perspective. Trends in Food Science & Technology, 17(10), 547-556 (2006). doi: http://dx.doi.org/10.1016/j.tifs.2006. 04.010

Sierra-Pallares, J., Marchisio, D. L., Parra-Santos, M. T., García-Serna, J., Castro, F., Cocero, M. J., A computational fluid dynamics study of supercritical antisolvent precipitation: Mixing effects on particle size. AIChE Journal, 58(2), 385-398 (2012). doi: 10.1002/aic.12594.

Silveira-Neto, A., Simulação de Grandes Escalas de Escoamentos Turbulentos Escola de Primavera de Transição e Turbulência. Turbulência. Rio de Janeiro: ABCM-Associação Brasileira de Ciências Mecânicas (2002). (In Portuguese).

Werling, J. O., Debenedetti, P. G., Numerical modeling of mass transfer in the supercritical antisolvent process: miscible conditions. The Journal of Supercritical Fluids, 18(1), 11-24 (2000). doi: http://dx.doi.org/10.1016/S0896-8446(00)00054-1

Wilcox, D. C., Turbulence Modeling for CFD La Canada. California DCW Industries (1993).

Yamamoto, S., Furusawa, T., Matsuzawa, R., Numerical simulation of supercritical carbon dioxide flows across critical point. International Journal of Heat and Mass Transfer, 54(4), 774-782 (2011). doi: http://dx.doi.org/10.1016/ j.ijheatmasstransfer. 2010.10.030